Nuclear Instruments and Methods in Physics Research A 780 (2015) 21–26

Contents lists available at ScienceDirect

Nuclear Instruments and Methods in Physics Research A

journal homepage: www.elsevier.com/locate/nima

Design of a high dynamic range photomultiplier base board for the BGO ECAL of DAMPE

Zhiyong Zhang, Yunlong Zhang*, Jianing Dong, Sicheng Wen, Changqing Feng, Chi Wang, Yifeng Wei, Xiaolian Wang, Zizong Xu, Shubin Liu

State Key Laboratory of Particle Detection and Electronics, University of Science and Technology of China, Hefei, Anhui 230026, China

ARTICLE INFO

Article history:
Received 7 March 2014
Received in revised form
9 January 2015
Accepted 11 January 2015
Available online 21 January 2015

Keywords:
ASIC
High dynamic range
Multi-dynode readout
VA32

ABSTRACT

A base board for photomultiplier tube (PMT) with multi-dynode readout has been developed for the BGO electromagnetic calorimeter (ECAL) of the Dark Matter Particle Explorer (DAMPE). In order to cover a high dynamic range of energy measurements, the signals are read out from different sensitive dynodes 2, 5, and 8 (Dy2, Dy5 and Dy8). The performance of this new type of base board is studied with a light-emitting diode (LED) system and cosmic rays. A wide measuring range from 0.5 to 1.0×10^5 MIPs can be achieved using the VA32 readout Application Specific Integrated Circuit (ASIC).

1. Introduction

Many experiments searching for direct or indirect evidence of dark matter have been carried out. An example of direct detection experiment is the LUX [1] underground experiment. Examples of indirect detection include the ATIC [2] balloon-borne experiment and the satellite-based experiments of PAMELA [3] and FERMI-LAT [4]. Exciting results from these experiments have been published [5–8]. DAMPE is an orbital experiment aiming at searching for dark matter by measuring the spectra of photons, electrons and positrons originating from deep space. The DAMPE detector is designed to cover a wide energy range, from 5 GeV to 10 TeV, with a good energy resolution of 1.5% at 800 GeV for photons and electrons, and will be one of the most precise detectors for energy measurement of these particles in an energy range from sub-TeV to tens-TeV.

The BGO ECAL is one of the key sub-detectors of the DAMPE. It contains 14 layers of BGO crystals (~31 radiation lengths). Each layer is composed of 22 BGO bars in dimensions of $2.5 \times 2.5 \times 60$ cm^3, with a PMT coupled on each side to collect scintillation light from the crystals. The layers of BGO bars are alternated in an orthogonal way to measure the deposited energy and shape of nuclear and electromagnetic showers developed in the crystals.

The VA32 ASIC, developed by IDE AS (Norway) [9], is adopted as the front-end electronics for the ECAL, and the version used for the prototype of the DAMPE detector is VA32HDR14.2. It is a 32-channel, low power ASIC for charge measurement, with a dynamic range from −3 pC to +13 pC, 1.8 μs shaping time and an intrinsic noise of about 0.5 fC RMS. The signal from a PMT of the ECAL is amplified and shaped through a VA32 chip. The analog output of the VA32 chip is then digitized by a 14-bit ADC. The dynamic range of the electronics system is $\sim 2 \times 10^2$, corresponding to an output of a PMT ranging from several tens fC to 12 pC.

2. Requirements

The energy of the particles ($\gamma, e^{\pm}$) measured at the DAMPE experiment varies from 5 GeV to 10 TeV. The energy deposit from a minimum ionizing particle (MIP) passing through a 2.5 cm thick BGO bar is about 23 MeV (1 MIP). A Geant4-based simulation indicates that, the maximum energy deposit in such a BGO bar is about 2 TeV from a 10 TeV electron, corresponding to about 10^5 MIPs. And a minimum measurable energy deposit of 0.5 MIPs is required for shower shape reconstruction with reasonable precision demanded by particle identification. Thus each single detection unit should cover energy measurements in a range from 0.5 MIPs to 10^5 MIPs, corresponding to a high dynamic range of 2×10^5.

To obtain such a wide dynamic range, a multi-dynode readout PMT base board is conceived. The basic idea is that different dynodes in a PMT are read out in parallel covering different energy ranges [10,11]. Large signals can be read out from the dynodes at early stages of the photoelectron multiplication chain, while small signals are read out from the dynodes at late stages. As the

* Corresponding author. Tel.: +86 055163603764.
E-mail address: ylzhang1@mail.ustc.edu.cn (Y. Zhang).

http://dx.doi.org/10.1016/j.nima.2015.01.036
0168-9002/

dynamic range of the electronics system is about $\sim 2 \times 10^2$, the PMTs with the multi-dynode readout base board are required to provide a dynamic range of 10^3, corresponding to a ratio of dynode gain up to 10^3. The design of the base board is the key component to achieve this high dynamic range, the details are presented in the following.

This paper focuses on the design and performance of the phototube base board. The specific requirements related to the operation of the apparatus in space such as the magnetic shielding of the photo detectors, the black glue potting for HV protection and light shading, the controls of outgassing of materials, would not be addressed in this document.

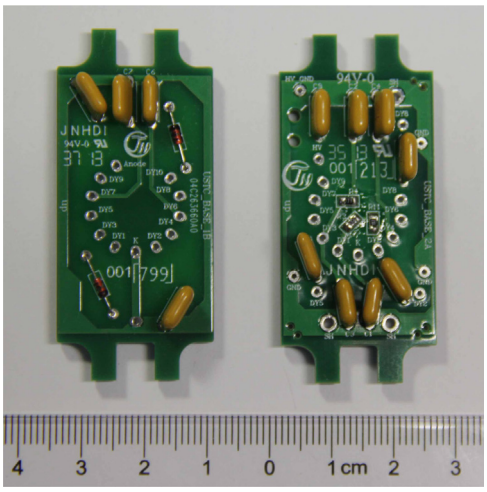

Fig. 1. Base board layout.

3. Design and test

3.1. The structural and thermal design

The base board contains two 2.5 mm thick flame-retardant FR-4 epoxy laminates, Fig. 1. Each laminate integrates four copper layers: the two surface layers are for routing, whilst the two inner layers, connected to the safety ground, are for conveying the heat produced on the base board [12]. Resistors are the only source of heat on the base board. Although the power is adequately small, less than 30 mW per PMT, we take it into account in the design, since PMTs are highly thermal-sensitive [13]. Due to the small installation space as a result of the dense arrangement of BGO crystals, the base board is divided into two stacked PCBs with an area of 4.4×2.5 cm^2. The two PCBs are directly soldered to PMTs pins.

3.2. Design of voltage-divider circuit

The PMTs chosen are of the type of R5610A-01 made by Hamamatsu [14], which has 10 stages of charge amplification. The voltage-divider circuit is designed as a pure resistors network with cascade voltage distribution (Fig. 2), producing almost the same voltage drop between the sequential dynodes, except for the one between the cathode and the first dynode, which is larger, in order to maximize the charge collection efficiency. The voltage drops across the last dynodes are also configured slightly larger for the purpose of assuring a good linearity by reducing the space charge effect (especially for Dy8). The

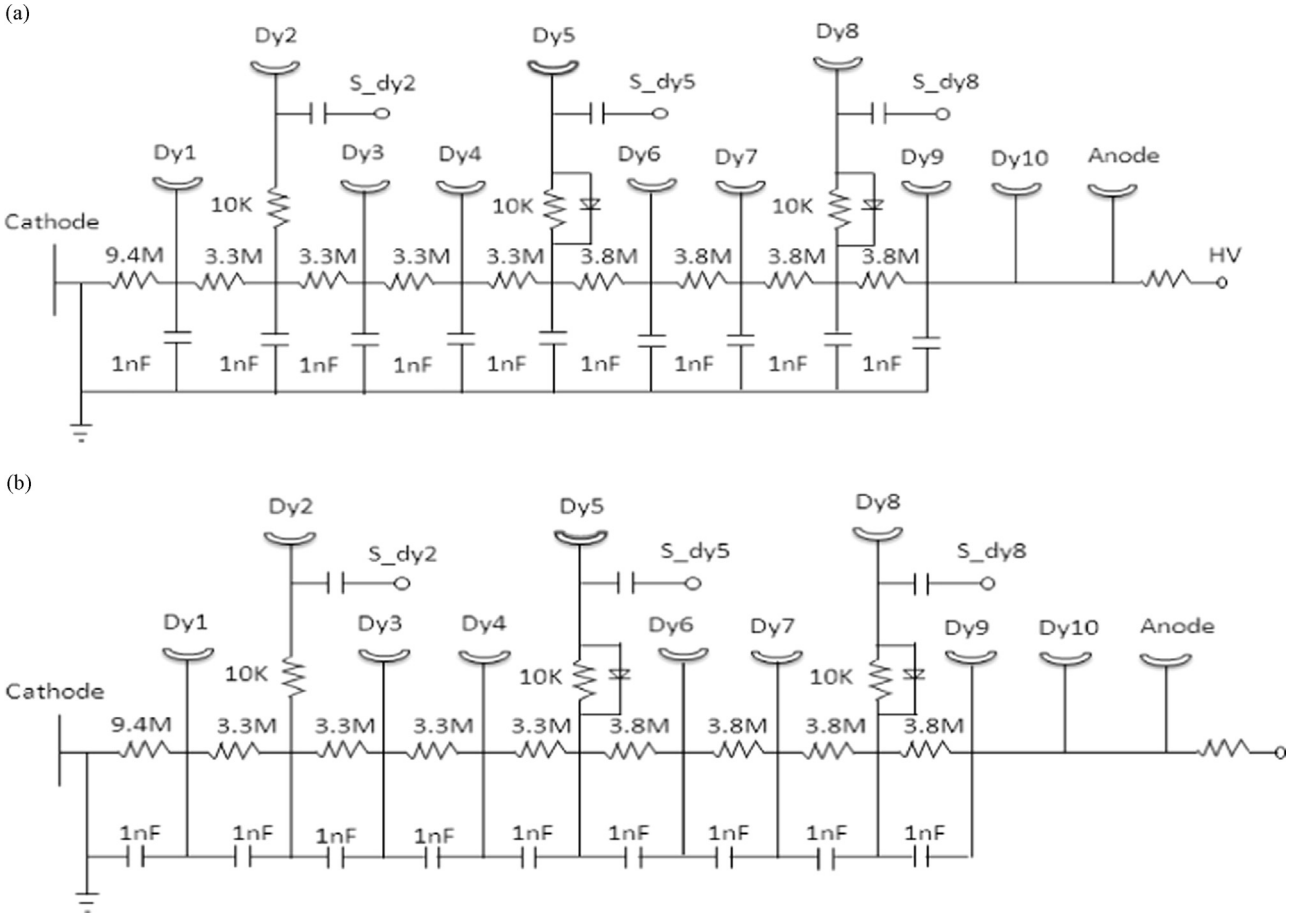

Fig. 2. The voltage-divider configured with two different filtering configurations. (a) Capacitors in parallel and (b) capacitors in series.

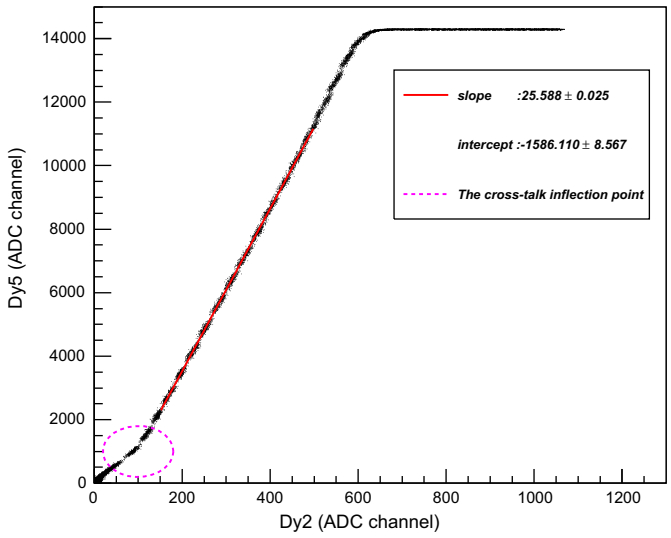

Fig. 3. Dy5 versus Dy2 with the crosstalk inflection point, that shows the Dy2 is disturbed (Capacitors in parallel).

linearity here refers to the correlations of readout dynodes, which will be discussed in the following section (Section 3.4). This is a typical high gain voltage-divider circuit which is suitable for the high dynamic range photometry [15,16].

In order to extend the photometry range, which is limited by the dynamic range of the VA32 chips, the signals from three dynodes, Dy2, Dy5 and Dy8 of the PMTs are recorded for the offline analysis. Two Schottky diodes (see Fig. 2) are used for discharging large signals of Dy5, Dy8 which would be picked up by the Dy2 readout due to crosstalk, and protecting the front-end amplifiers from very large signals. Cables are soldered to the base board to supply high voltage and extract signals from the dynodes.

Two designs of filtering capacitance networks, series and parallel as shown in Fig. 2(a) and (b), respectively, have been scrutinized in terms of gain, stability and crosstalk. The typical voltage (across each capacitor) of the series connection is less than 200 V, ensuring a safe operation of the device. The capacitors in the parallel design are subjected to a maximal voltage of 1000 V, requiring big large-size capacitors. But the parallel configuration provides better filtering performance as will be discussed in Section 3.3.

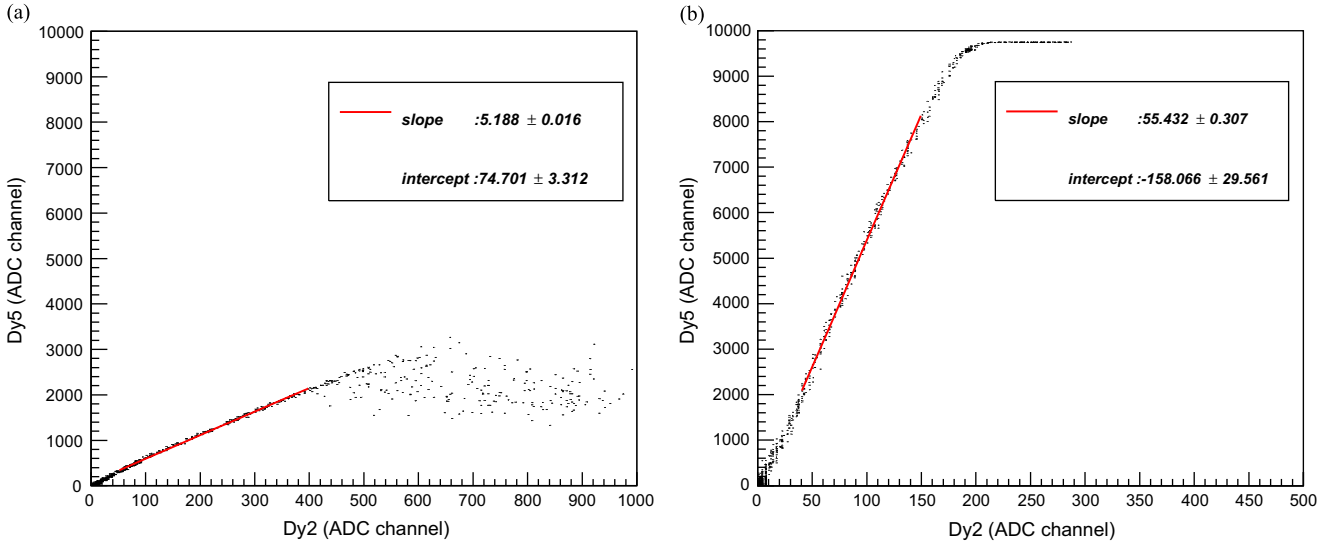

Fig. 4. Dy5 versus Dy2. (a) Capacitors in series and (b) capacitors in parallel.

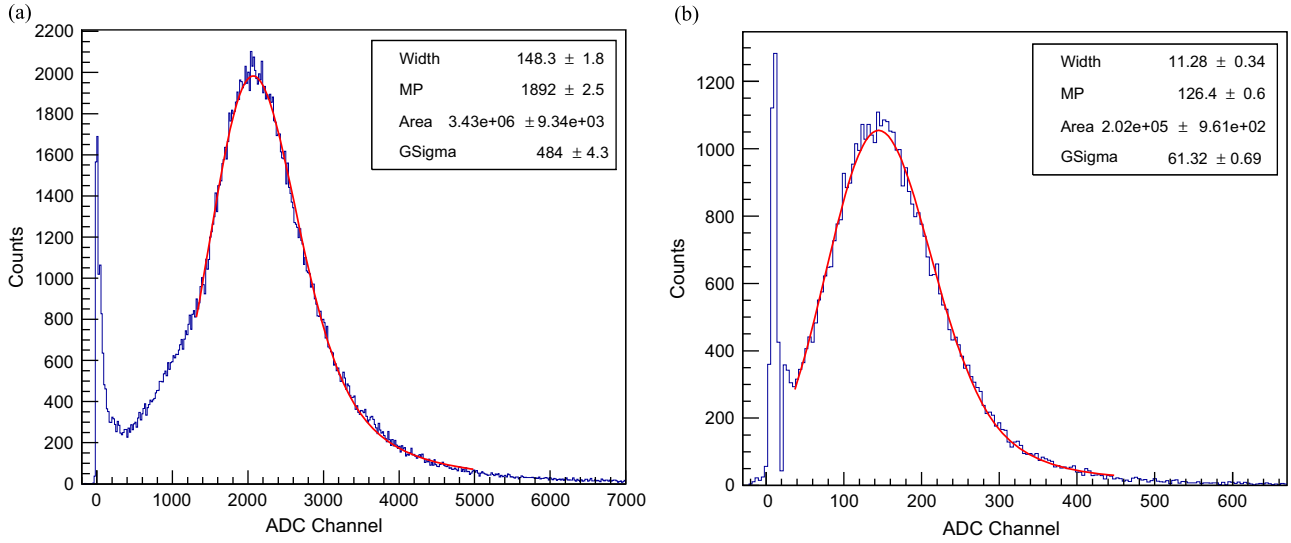

Fig. 5. (Cosmic muon) MIPs spectrum (with pedestal peak). (a) Raw MIPs. and (b) after adding attenuation filter.

3.3. Crosstalk between dynodes

A LED test system was set up to study the performance of the base board described above [17]. The LED is driven by a pulse generator, and the light pulses emitted by the LED are fanned out to the PMTs through optical fibers. The outputs of the PMTs are digitized after amplification and shaping with the VA32 chips. Dy2 signal is small, and, as a consequence, it is subjected to disturbances. In the case of the parallel capacitor design, the output of Dy8 induces a positive crosstalk signal in Dy2, which, in turn, results in decreasing the ratio Dy5/Dy2. Fig. 3 shows the correlation between Dy5 charge and Dy2 charge. There is a point in the correlation where the charge ratio of Dy5 to Dy2 gets increased suddenly (at Dy2 charge of around 200 ADC counts in Fig. 3). This is where the bypass diode to Dy8 is turned on leading to a much smaller crosstalk from Dy8 to Dy2. Additional reduction in crosstalk was achieved by minimizing the capacitive coupling between dynodes:

- Keeping components and lining associated with Dy2 as far as possible from the later dynodes on the base board.
- Using well shielded cables for the signal extraction of the readout dynodes.
- Sending the signals from three dynodes of the same PMT to different V32 chips.

Fig. 4(b) shows the performance of the parallel design after all these corrective actions against crosstalk have been taken.

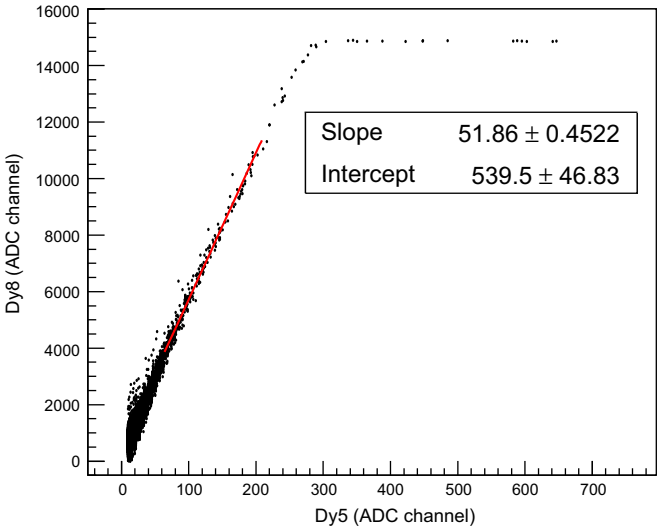

Fig. 6. Relation of Dy8 and Dy5 (with cosmic-ray shower events).

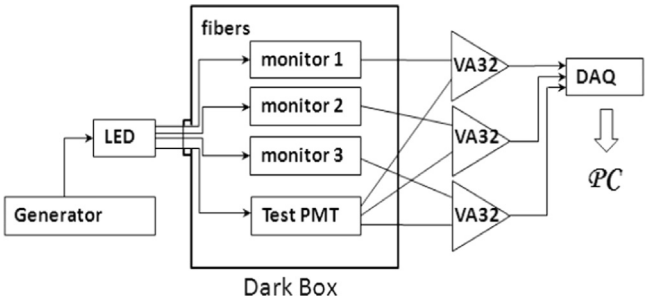

Fig. 7. Test setup for the characteristics of the PMT's dynamic range.

3.4. Comparison of the two designs

The performance was studied under the same test conditions (HV, PMT, DAQ system) with the two different filtering capacitor configurations. The ratio between Dy5 and Dy2 is shown, Fig. 4. Dy2 picks up extra charges, due to crosstalk from the latter dynodes, when using the capacitors in series configuration, Fig. 4(a). The ratio is ~10 times smaller than that of the configuration with the capacitors in parallel, Fig. 4(b). The obtained result supports the choice of the configuration with the filtering capacitors in parallel. The poorer performance of the series configuration is consequent to the fact that the signal, while driven to ground, is also injected to the dynodes which sit on its path.

4. Results

4.1. Test with cosmic rays

Cosmic muons were used to calibrate the MIPs response at ground level. The PMTs with the base board described above were used for photon collection. Fig. 5(a) shows a typical MIPs energy spectrum recorded by the Dy8 (charges of Dy2 and Dy5 are too small for MIP energy deposit) readout. The light yield of BGO crystals is rather high. So the light from the BGO crystals needs to be attenuated before entering the PMTs in order to reach an energy up to ~2 TeV before the electronics system gets saturated. The light is attenuated through a filter placed between BGO crystals and PMTs. The attenuation is tuned so that the response of a single BGO crystal

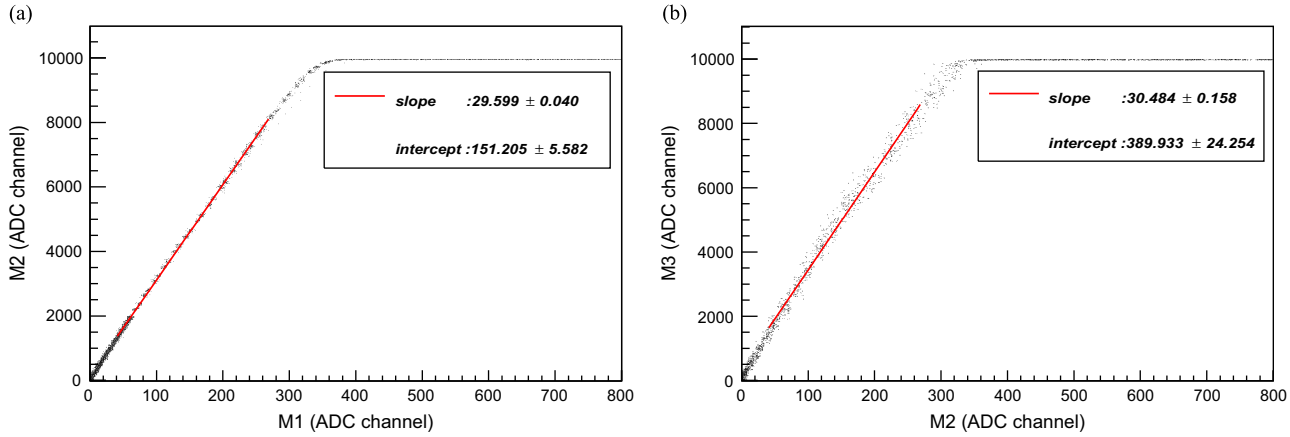

Fig. 8. Reciprocal monitors correlations. (a) Monitor 2 versus monitor 1 and (b) monitor 3 versus monitor 2.

bar to 1 MIP is about 100 fC. Fig. 5(b) shows the MIPs energy spectrum after the light from BGO crystals was attenuated.

The BGO ECAL provides trigger signals for the DAMPE experiment, which requires that the PMT signals of the same layer of BGO crystals should be as uniform as possible. A good uniformity in response over a single BGO layer is achieved by adjusting the light attenuation on a channel-by-channel basis.

Cosmic ray shower events were used to calibrate the charge ratio of Dy8 and Dy5. Compared with the LED test (Fig. 4(b)), this calibration with BGO crystals was more representative of the actual experiment. The result is shown in Fig. 6, the Dy5 varies from 0 to 300 ADC counts corresponding to 0 to saturation of the Dy8 with the different energy deposit of shower events. The clear fitted correlation will be used for energy reconstruction when the electronics of Dy8 gets saturated. Since the energy deposit (in a BGO bar) of shower events can only cover the dynamic range of Dy8, the correlation of Dy5 and Dy2 can only be calibrated by high energy particle beam or on orbit.

4.2. Dynamic range

To verify the high dynamic range of the PMT with the designed base board, we performed test of the readout system using three reference PMTs with different sensitivities (M3, M2 and M1, in ascending order of sensitivity). The light from a pulsed LED was split into 4 fibers (Fig. 7). The pulse driving the LED was shaped, so that the output light from the LED had a similar shape to that of actual scintillation light from a BGO crystal. The pulse height was programmed so that the light to the PMTs was able to cover the full range of the tested PMT with the base board. Though the absolute flux of the light injected to PMTs is difficult to estimate, the relative flux, called Equivalent Flux (E_f), could be determined using the ADC counts of the associated-reference PMTs, through the following formula:

$$E_f = \begin{cases} A_{M3} & \text{if } A_{M3} < A_{Sat} \\ A_{M2} \cdot S_{M3,M2} + I_{M3,M2} & \text{if } A_{M3} > A_{Sat}, A_{M2} < A_{Sat} \\ (A_{M1} \cdot S_{M2,M1} + I_{M2,M1}) \cdot S_{M3,M2} + I_{M3,M2} & \text{if } A_{M2} > A_{Sat} \end{cases}$$

where A_{M1}, A_{M2}, A_{M3} are the digital ADC counts of the monitors, and A_{Sat} is the maximum ADC channel of the electronics before the saturation effect becomes significant (8000 for this case). $S_{M3,M2}$, $S_{M2,M1}$ and $I_{M3,M2}$, $I_{M2,M1}$ are the slopes and intercepts obtained by fitting the correlation of the scattering plots with a linear function (Fig. 8(a,b)). According to their sensitivities, M3 was used to calibrate Dy8. A_{M3} is directly taken as the E_f until it reaches A_{Sat}, and then A_{M2}, takes over as the new references with the increase of the light flux. This is then followed by A_{M1}.

The outputs of tested PMT are plotted as a function of E_f in Fig. 9. Since 1 MIP of the tested PMT has been set at ~100 fC (Fig. 5(b)), according to the correlation of the monitors and tested PMT, 1 MIP energy deposit is equal to ~71 units of E_f. The values of E_f are also converted to energy deposits in units of MIP (top coordinate of Fig. 9). The results show that Dy8, Dy5 and Dy2 do provide a linear response in the whole dynamic range, which corresponds to BGO energy deposits of 0.5–1.0 × 10^2 MIPs, 30–3.0 × 10^3 MIPs, and 1.0 × 10^3–1.0 × 10^5 MIPs, respectively.

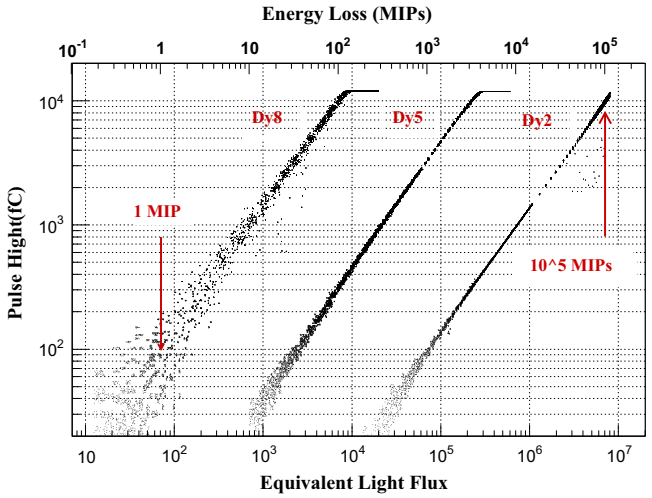

Fig. 9. Outputs of three dynodes (fC) respond to the Equivalent Light Fluxes (E_f) and the Energy Loss (with "MIPs" unit).

5. Production

In total, 624 base boards were produced and installed on PMTs (among which 616 were used in a full-size BGO ECAL prototype). The 624 PMTs with the base boards were tested with the LED system.

The dynamic ranges of all PMTs meet the requirement of 10^3 (shown in Fig. 10(a)). Both Dy5 and Dy8 are used to generate trigger signals. Therefore, the slopes of Dy8/Dy5 (Fig. 10(b)) need

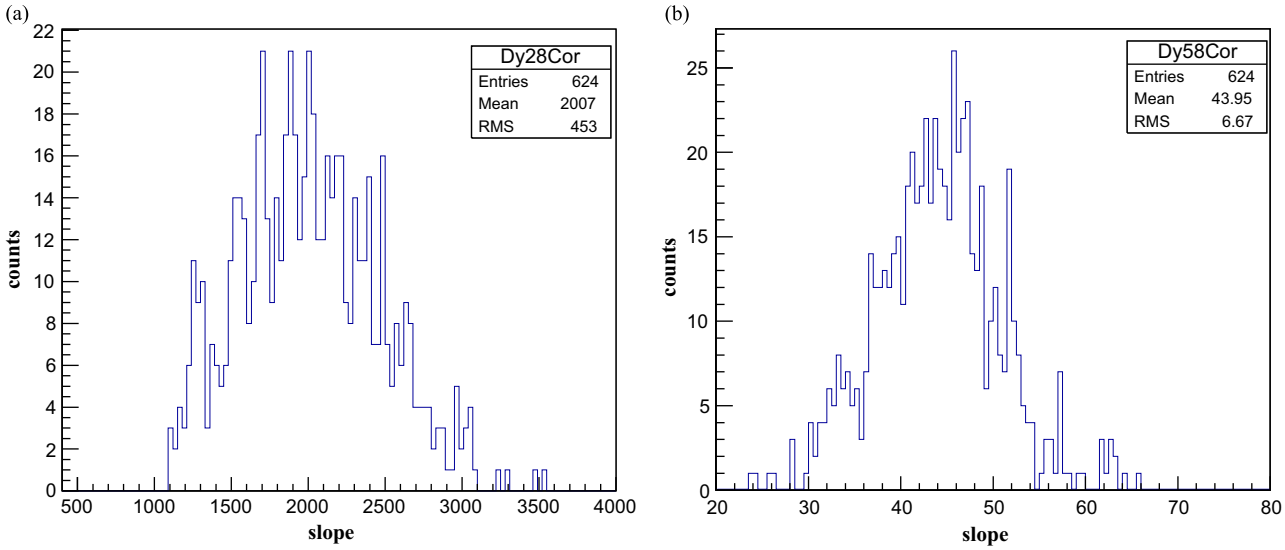

Fig. 10. Distribution of the relative gains between the readout dynodes. (a) Dy8 versus Dy2 and (b) Dy8 versus Dy5.

to be close for trigger layers in order to use a common threshold. According to these results, the PMTs with similar slopes are arranged to compose the same BGO layers. Some PMTs with anomalous slopes are rejected. Once the installation of 14 layers of PMTs and crystals finished, a long-term test with cosmic rays was carried out for calibration and performance studies. The spread of the slopes of the different base boards is a bit large, it should be no matter, since the slopes will be sufficiently calibrated on the ground (Dy8/Dy5 by cosmic rays and Dy5/Dy2 by high energy particle beams) and on orbit in the future.

6. Conclusions

A multi-dynode readout base board has been designed and extensively tested. The charge ratios of Dy8 to Dy5 and Dy5 to Dy2 have been measured to be around 30 and 60. A wide dynamic range of a single BGO+PMT+base board unit for energy measurement, from several MeV to 2 TeV (corresponding to sub-GeV to 10 TeV of incident electrons), has been verified by using an LED system. The performance of all 624 base boards was tested with the LED and cosmic rays. The tests have shown that the base boards satisfy all technical requirements on them. Further tests studies, such as the particle beam tests, will be carried out in the incoming months.

Acknowledgments

This work was supported by the Chinese 973 Program, Grant No. 2010CB833002, the Strategic Priority Research Program on Space Science of the Chinese Academy of Science, Grant No. XDA04040202-4. The authors wish to thank Professor Guangshun Huang, Professor Jianbei Liu and Dr. Yang Liu for their careful proofreading, thank Mr. Gordon Munro and Mr. Liang Guan for language revision.

References

[1] D.S. Akerib, et al., Nuclear Instruments and Methods in Physics Research A 704 (2013) 111.
[2] T.G. Guzik, et al., Proceeding of SPIE 2806 122 (October (18)) (1996).
[3] P. Picozza, R. Sparvoli, Nuclear Instruments and Methods in Physics Research A 623 (2010) 672.
[4] W.B. Atwood, et al., The Astrophysical Journal 697 (June (1)) (2009) 1071.
[5] F. Aharonian, et al., Physical Review Letters 101 (2008) 261104.
[6] J. Chang, et al., Nature 456 (2008) 362.
[7] O. Adriani, et al., Nature 458 (2009) 607.
[8] A.A. Abdo, et al., Physical Review Letters 102 (2009) 181101.
[9] Integrated Detector Electronics AS (IDEAS), VA32HDR14.2-V1R1 datasheet, ⟨http://www.ideas.no⟩.
[10] Y.L. Zhang, et al., CPC (HEP&NP) 36 (1) (2012) 71.
[11] B. Genolini, et al., Nuclear Instruments and Methods in Physics Research A 504 (2003) 240.
[12] M. Ameri, et al., Nuclear Instruments and Methods in Physics Research A 550 (2005) 559.
[13] S. Ogio, et al., in: Proceeding of the 31st ICRC, Lodz, 2009.
[14] Photomultiplier tubes and related products, PMT_TPMZ0001E01, Document library, ⟨http://www.hamamatsu.com/resources/pdf/etd/PMT_TPMZ0001E01.pdf⟩.
[15] Photomultiplier tubes basics, ⟨http://particle.korea.ac.kr/lab/cata_basic.pdf⟩.
[16] Photomultiplier tubes basics and applications, PMT_handbook_v3aE, Document library, ⟨http://www.hamamatsu.com/resources/pdf/etd/PMT_handbook_v3aE.pdf⟩.
[17] M. Friend, et al., Nuclear Instruments and Methods in Physics Research A 676 (2012) 66.